

Mass calculations of light quarkonium, exotic $J^{PC} = 0^{+-}$ hybrid mesons from Gaussian sum rules

J. Ho,^{*} R. Berg,[†] and T. G. Steele[‡]

*Department of Physics and Engineering Physics, University of Saskatchewan,
Saskatoon, SK, S7N 5E2, Canada*

Wei Chen[§]

School of Physics, Sun Yat-Sen University, Guangzhou 510275, China

D. Harnett^{||}

Department of Physics, University of the Fraser Valley, Abbotsford, BC, V2S 7M8, Canada



(Received 2 July 2018; published 28 November 2018)

We extend previous calculations of leading-order correlation functions of spin-0 and spin-1 light quarkonium hybrids to include QCD condensates of dimensions five and six, with a view to improving the stability of QCD sum-rules analyses in previously unstable channels. Based on these calculations, prior analyses in the literature, and its experimental importance, we identify the exotic $J^{PC} = 0^{+-}$ channel as the most promising for detailed study. Using Gaussian sum rules constrained by the Hölder inequality, we calculate masses of light (nonstrange and strange) quarkonium hybrid mesons with $J^{PC} = 0^{+-}$. A model-independent analysis of the hadronic spectral function indicates that there is distributed resonance strength in this channel. Hence, we study two hadronic models with distributed resonance strength: a single wide resonance model and a double narrow resonance model. The single wide resonance model is disfavored as it leads to an anomalously large resonance width (greater than 1 GeV). The double narrow resonance model yields excellent agreement between QCD and phenomenology: in both nonstrange and strange cases, we find hybrid masses of 2.60 GeV and 3.57 GeV.

DOI: [10.1103/PhysRevD.98.096020](https://doi.org/10.1103/PhysRevD.98.096020)

I. INTRODUCTION

It has long been conjectured that hadrons could exist beyond the conventional quark model of quark-antiquark ($q\bar{q}$) mesons and three-quark (qqq , $\bar{q}\bar{q}\bar{q}$) baryons. In particular, color-singlet hybrid mesons consisting of a quark, antiquark, and explicit gluonic degree of freedom have a long history [1]. While evidence of hadronic structures outside of the conventional model has been accumulating with experimental observations and confirmations of tetraquarks [2–4] and pentaquarks [5], an experimental confirmation of hybrid mesons has eluded observation. Designed to search for light hybrid mesons

(particularly those with exotic J^{PC} that do not exist in the conventional quark model), the GlueX experiment at Jefferson Lab [6] is currently underway, and is anticipated to give crucial insight into the existence and structure of light hybrids.

The characterization of light hybrid states within the framework of QCD is important. Identifying the spectrum of the lightest hybrid supermultiplet ($J^{PC} \in \{1^{--}, (0, 1, 2)^{--}\}$, where the $q\bar{q}$ are in an S -wave configuration) and the neighboring larger supermultiplet ($J^{PC} \in \{0^{+-}, 1^{+-}, 2^{+-}, 3^{+-}, (0, 1, 2)^{++}\}$, where the $q\bar{q}$ are in a P -wave configuration) is of particular interest from an experimental perspective, and is aligned with the mandate of the GlueX experiment [6]. There have been numerous studies done on light quark hybrids covering a range of quantum numbers using QCD Laplace sum rules (LSRs) [7–23], lattice QCD [24,25], the Schwinger-Dyson formalism [26–28], the flux tube model [29,30], and the MIT bag model [31,32]. In particular, Ref. [11] contains a comprehensive LSRs analysis of light hybrids for all J^{PC} with $J \in \{0, 1\}$ that takes into account condensates up to dimension four (i.e., 4d). Analyses of the 0^{++} , 0^{--} , 1^{++} , and 1^{--} sectors were stable; analyses of the 0^{+-} ,

^{*}j.ho@usask.ca
[†]rtb867@mail.usask.ca
[‡]tom.steele@usask.ca
[§]chenwei29@mail.sysu.edu.cn
^{||}derek.harnett@ufv.ca

Published by the American Physical Society under the terms of the Creative Commons Attribution 4.0 International license. Further distribution of this work must maintain attribution to the author(s) and the published article's title, journal citation, and DOI. Funded by SCOAP³.

0^{+-} , 1^{+-} , and 1^{++} sectors were unstable. Expected to be the lightest hybrid with exotic quantum numbers, the 1^{+-} has been the subject of much additional study. Reference [15] contains a (error-free) 1^{+-} hybrid correlator that includes condensates up to 6d. By analyzing lower-weight LSRs than those used in [11], the authors arrived at a stable mass prediction. Subsequently, a variety of improvements (e.g., radiative corrections and higher dimension condensates) were included in the 1^{+-} hybrid correlator, and the LSRs analyses were updated accordingly [17–22]. In the LSRs analysis of [16], a stable mass prediction for the 0^{+-} was found using a current different from that of [11]. The only stable LSRs analysis of the 0^{+-} channel [13] used higher-dimension currents and required estimation of the low-energy theorem term from other channels, introducing multiple sources of theoretical uncertainty. Thus, further QCD sum rules studies of the 0^{+-} channel are necessary.

In [33–36], it was found that the inclusion of higher-dimension condensates stabilized previously unstable LSRs analyses from [11] of hybrids containing heavy quarks. Therefore, in Sec. II we provide a systematic computation of leading-order (LO) 5d and 6d condensate contributions for all light quarkonium hybrids of spin-zero and spin-one. Unfortunately, as discussed in Sec. III, these higher-dimension condensates do not stabilize the unstable light hybrid LSRs analyses as they do for heavy hybrids. However, in [11], it was proposed that the instability in the LSRs might be resolved by accounting for finite width effects, an issue also raised in [13]. As we show in Sec. V, a model-independent analysis of the 0^{+-} hadronic spectral function indicates that there is distributed (as opposed to concentrated) resonance strength in this channel. To explore width effects and the possibility of excited states, we depart from previous LSRs methods. Gaussian sum rules (GSRs) [37] are sensitive probes of width effects and both ground and excited states, and have been shown to be a powerful and versatile analysis methodology [38–41]. In particular, the QCD sum-rules paradigm of the ρ meson was used to benchmark and validate these GSR methodologies [38]. Thus, in this article, we use GSRs to investigate the possibility of distributed resonance strength in the exotic 0^{+-} light hybrid channel.

In Sec. II, we calculate LO spin-0 and spin-1 correlation functions of light quarkonium hybrid currents, including condensates up to 6d. Section III includes a review of the GSRs formalism, and a theoretical constraint on the GSRs based on the Hölder inequality is developed in Sec. IV. The GSRs analysis methodology and results for the 0^{+-} channel are presented in Sec. V with concluding remarks in Sec. VI.

II. HYBRID CURRENTS AND CORRELATION FUNCTIONS

To investigate light quarkonium hybrids, we use currents of the form

TABLE I. The J^{PC} combinations probed through different choices of Γ^ν and $\mathcal{G}_{\mu\nu}^a$ in (1).

Γ^ν	$\mathcal{G}_{\mu\nu}^a$	J^{PC}
γ^ν	$G_{\mu\nu}^a$	$0^{++}, 1^{--}$
γ^ν	$\tilde{G}_{\mu\nu}^a$	$0^{-+}, 1^{+-}$
$\gamma^\nu\gamma_5$	$G_{\mu\nu}^a$	$0^{--}, 1^{+-}$
$\gamma^\nu\gamma_5$	$\tilde{G}_{\mu\nu}^a$	$0^{+-}, 1^{--}$

$$j_\mu = g_s \bar{q} \Gamma^\nu t^a \mathcal{G}_{\mu\nu}^a q, \quad (1)$$

where q is a light (nonstrange or strange) quark field and t^a are generators of the fundamental representation of $SU(3)$. Each combination of $\mathcal{G}_{\mu\nu}^a \in \{G_{\mu\nu}^a, \tilde{G}_{\mu\nu}^a = \frac{1}{2} \epsilon^{\mu\nu\rho\sigma} G_{\rho\sigma}^a\}$ and Dirac structure Γ^ν together corresponds to particular values of J^{PC} [11,15]; these combinations are summarized in Table I.

For each current (1), we calculate and decompose a diagonal correlation function as follows:

$$\Pi_{\mu\nu}(q) = i \int d^4x e^{iq \cdot x} \langle 0 | \tau j_\mu(x) j_\nu^\dagger(0) | 0 \rangle \quad (2)$$

$$= \frac{q_\mu q_\nu}{q^2} \Pi^{(0)}(q^2) + \left(\frac{q_\mu q_\nu}{q^2} - g_{\mu\nu} \right) \Pi^{(1)}(q^2) \quad (3)$$

where $\Pi^{(0)}$ probes spin-0 states and $\Pi^{(1)}$ probes spin-1 states.

The calculation of (2) is performed in the framework of the operator product expansion (OPE),

$$\langle \Omega | \tau \{ \mathcal{O}(x) \mathcal{O}(0) \} | \Omega \rangle = \sum_n C_n(x) \langle \Omega | : \mathcal{O}_n(0) : | \Omega \rangle. \quad (4)$$

In (4), the vacuum expectation value (VEV) of a time-ordered, non-local product of composite operators is expanded in a series, each term of which is a product of a perturbative Wilson coefficient $C_n(x)$ and a nonzero VEV of a local composite operator $\mathcal{O}_n(0)$, i.e., a condensate. The condensates parametrize the nonperturbative nature of the QCD vacuum, and we include in our correlator calculations the following set:

$$\langle \bar{q}q \rangle = \langle \bar{q}_i^\alpha q_i^\alpha \rangle \quad (5)$$

$$\langle \alpha G^2 \rangle = \langle \alpha_s G_{\mu\nu}^a G_{\mu\nu}^a \rangle \quad (6)$$

$$\langle g \bar{q} \sigma G q \rangle = \langle g_s \bar{q}_i^\alpha \sigma_{ij}^{\mu\nu} \lambda_{\alpha\beta}^a G_{\mu\nu}^a q_j^\beta \rangle \quad (7)$$

$$\langle g^3 G^3 \rangle = \langle g_s^3 f^{abc} G_{\mu\nu}^a G_{\nu\rho}^b G_{\rho\mu}^c \rangle \quad (8)$$

$$\langle \bar{q}q\bar{q}q \rangle = \langle \bar{q}_i^\alpha q_i^\alpha \bar{q}_j^\beta q_j^\beta \rangle, \quad (9)$$

respectively the 3d quark condensate, the 4d gluon condensate, the 5d mixed condensate, the 6d gluon

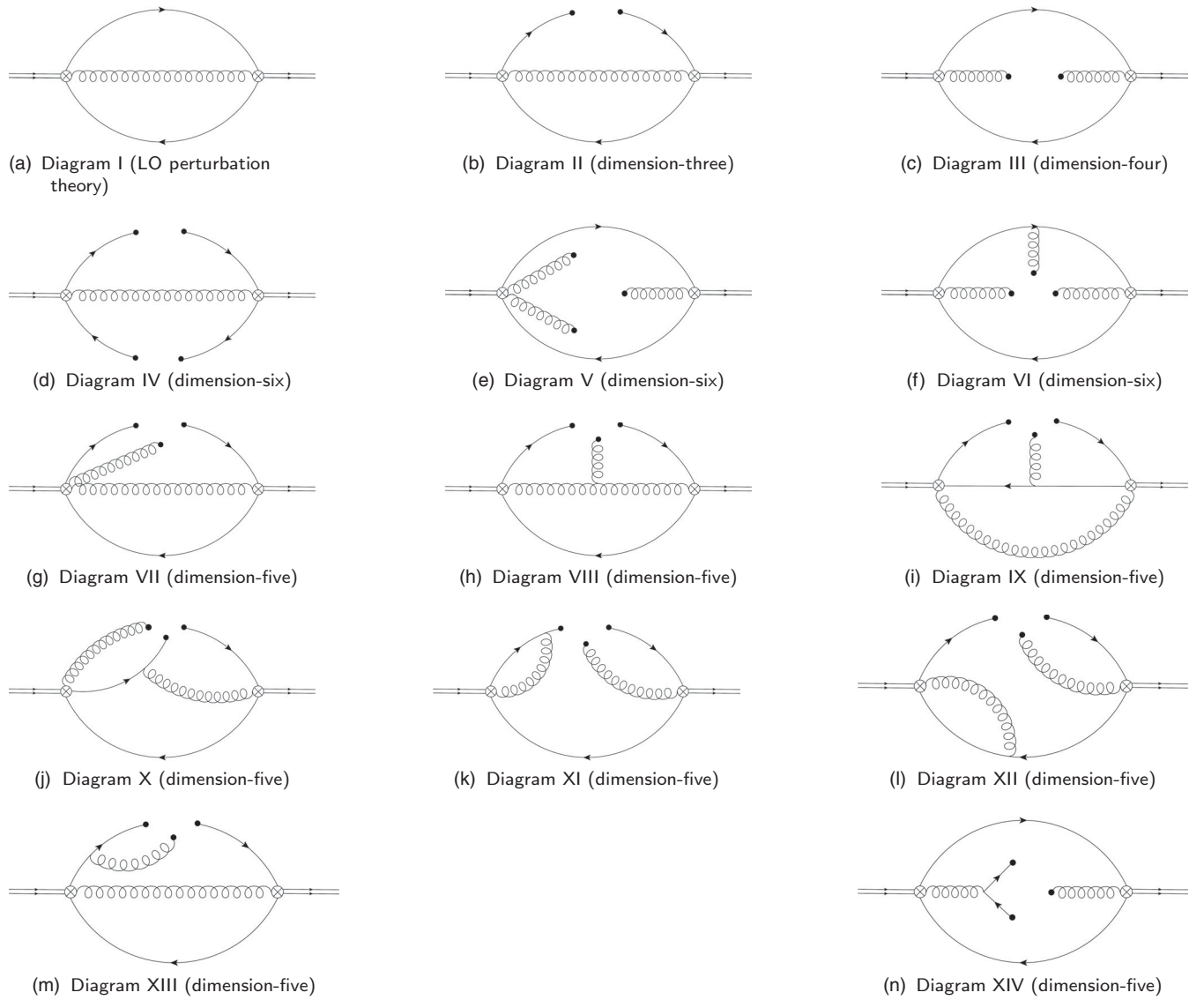


FIG. 1. The Feynman diagrams calculated for the correlator (2). Feynman diagrams were created using JAXODRAW [43].

condensate, and the 6d quark condensate. In (5)–(9), superscripts on quark fields are color indices whereas subscripts are Dirac indices and $\sigma^{\mu\nu} = \frac{i}{2}[\gamma^\mu, \gamma^\nu]$. Regarding Wilson coefficients, we consider LO calculations in α_s , and we compute $\mathcal{O}(m^2)$ light quark mass corrections to perturbation theory as a way to distinguish between the nonstrange- and strange-flavored cases, similar to [42]. Also, the values of (5), (7), and (9) depend on whether the light quarks are nonstrange or

strange. The diagrams representative of the correlation function calculation are displayed in Figure 1. We use dimensional regularization in $D = 4 + 2\epsilon$ dimensions at $\overline{\text{MS}}$ renormalization scale μ . The program TARCER [44] is utilized to reduce the resulting integrals to a selection of well-known master integrals using the Tarasov recurrence relations [45,46].

All of the correlators defined between (1) and Table I can be written in general as

$$\begin{aligned} \Pi(q^2) = & \alpha_s (A_1 q^6 + A_2 m^2 q^4) \left\{ \log\left(\frac{-q^2}{\mu^2}\right) + \frac{1}{2\epsilon} \right\} + (A_4 q^2 \langle \alpha G^2 \rangle + \alpha_s (A_3 q^2 m \langle \bar{q}q \rangle + A_5 \langle \bar{q}q \rangle^2 + A_6 \langle g^3 G^3 \rangle + A_7 m \langle g\bar{q}\sigma Gq \rangle)) \\ & \times \left\{ \log\left(\frac{-q^2}{\mu^2}\right) + \frac{1}{\epsilon} \right\} + \alpha_s (B_1 q^6 + B_2 m^2 q^4 + B_3 q^2 m \langle \bar{q}q \rangle + B_4 q^2 \langle \alpha G^2 \rangle + B_5 \langle \bar{q}q \rangle^2 + B_6 \langle g^3 G^3 \rangle + B_7 m \langle g\bar{q}\sigma Gq \rangle) \end{aligned} \quad (10)$$

TABLE II. Coefficients of the logarithmic and divergent terms of the perturbative and condensate contributions to the correlation function (10) for the J^{PC} summarized in Table I.

	0^{++}	1^{-+}	0^{--}	1^{+-}	0^{-+}	1^{++}	0^{+-}	1^{--}
A_1	$-\frac{1}{480\pi^3}$	$-\frac{1}{240\pi^3}$	$-\frac{1}{480\pi^3}$	$-\frac{1}{240\pi^3}$	$-\frac{1}{480\pi^3}$	$-\frac{1}{240\pi^3}$	$-\frac{1}{480\pi^3}$	$-\frac{1}{240\pi^3}$
A_2	0	$\frac{1}{12\pi^3}$	$\frac{1}{16\pi^3}$	$\frac{5}{48\pi^3}$	0	$\frac{1}{12\pi^3}$	$\frac{1}{16\pi^3}$	$\frac{5}{48\pi^3}$
A_3	$\frac{1}{3\pi}$	$-\frac{2}{9\pi}$	$-\frac{1}{3\pi}$	$-\frac{4}{9\pi}$	$\frac{1}{3\pi}$	$-\frac{2}{9\pi}$	$-\frac{1}{3\pi}$	$-\frac{4}{9\pi}$
A_4	$\frac{1}{24\pi}$	$-\frac{1}{36\pi}$	$\frac{1}{24\pi}$	$-\frac{1}{36\pi}$	$-\frac{1}{24\pi}$	$\frac{1}{36\pi}$	$-\frac{1}{24\pi}$	$\frac{1}{36\pi}$
A_5	0	0	0	0	0	0	0	0
A_6	0	0	0	0	0	0	0	0
A_7	$\frac{1}{9\pi}$	0	$\frac{11}{72\pi}$	$-\frac{19}{72\pi}$	$-\frac{1}{9\pi}$	0	$-\frac{11}{72\pi}$	$\frac{19}{72\pi}$

TABLE III. Coefficients of the finite terms of the perturbative and condensate contributions to the correlation function (10) for the J^{PC} summarized in Table I.

	0^{++}	1^{-+}	0^{--}	1^{+-}	0^{-+}	1^{++}	0^{+-}	1^{--}
B_1	$\frac{97}{19200\pi^3}$	$\frac{39}{3200\pi^3}$	$\frac{97}{19200\pi^3}$	$\frac{39}{3200\pi^3}$	$\frac{19}{6400\pi^3}$	$\frac{77}{9600\pi^3}$	$\frac{19}{6400\pi^3}$	$\frac{77}{9600\pi^3}$
B_2	$\frac{1}{32\pi^3}$	$-\frac{7}{32\pi^3}$	$-\frac{55}{384\pi^3}$	$-\frac{109}{384\pi^3}$	$\frac{1}{32\pi^3}$	$-\frac{13}{96\pi^3}$	$-\frac{31}{384\pi^3}$	$-\frac{23}{128\pi^3}$
B_3	$-\frac{1}{2\pi}$	$\frac{7}{27\pi}$	$\frac{1}{6\pi}$	$\frac{17}{27\pi}$	$\frac{1}{6\pi}$	$-\frac{5}{27\pi}$	$-\frac{1}{2\pi}$	$-\frac{7}{27\pi}$
B_4	$-\frac{13}{144\pi}$	$\frac{11}{216\pi}$	$-\frac{13}{144\pi}$	$\frac{11}{216\pi}$	$-\frac{5}{144\pi}$	$\frac{7}{216\pi}$	$-\frac{5}{144\pi}$	$\frac{7}{216\pi}$
B_5	$-\frac{4\pi}{3}$	$\frac{4\pi}{9}$	$\frac{4\pi}{3}$	$-\frac{4\pi}{9}$	0	$-\frac{8\pi}{9}$	0	$-\frac{8\pi}{9}$
B_6	$-\frac{1}{192\pi^2}$	$\frac{1}{192\pi^2}$	$-\frac{1}{192\pi^2}$	$\frac{1}{192\pi^2}$	$\frac{5}{192\pi^2}$	$-\frac{5}{192\pi^2}$	$\frac{5}{192\pi^2}$	$-\frac{5}{192\pi^2}$
B_7	$-\frac{461}{1728\pi}$	$-\frac{83}{1728\pi}$	$-\frac{731}{1728\pi}$	$\frac{1019}{1728\pi}$	$-\frac{217}{1728\pi}$	$\frac{265}{1728\pi}$	$\frac{41}{1728\pi}$	$\frac{71}{1728\pi}$

where we have suppressed the superscript (J) on the left-hand side. The coefficients A_i and B_j contained in (10) are given in Tables II and III respectively. We note that, as Diagram IV has no loops, A_5 is trivially zero. In all channels, perturbation theory, the 3d quark condensate term, and the 4d gluon condensate term were benchmarked against [11]. The 0^{--} and 1^{-+} correlators were benchmarked against [15].

III. QCD SUM RULES

Each function $\Pi^{(J)}(q^2)$ defined in (3) satisfies a dispersion relation at Euclidean momentum $Q^2 = -q^2 > 0$,

$$\Pi(Q^2) = Q^8 \int_{t_0}^{\infty} \frac{1}{\pi} \frac{\text{Im}\Pi(t)}{t^4(t+Q^2)} dt + \dots, \quad (11)$$

where we have again suppressed the superscript (J). In (11), t_0 is a hadron production threshold and \dots are subtraction constants, together a third degree polynomial in Q^2 . Equation (11) connects theoretical predictions of QCD, i.e., $\Pi(Q^2)$ on the left-hand side, to properties of hadrons contained in $\text{Im}\Pi(t)$, the hadronic spectral function, on the right-hand side.

Regarding (11), to eliminate subtraction constants and to accentuate the low-energy region of the integral on the right-hand side, some transformation is typically applied. A popular choice is to formulate unsubtracted LSRs of (usually nonnegative) integer weight k ,

$$\mathcal{R}_k(M_B) = M_B^2 \lim_{\substack{N, Q^2 \rightarrow \infty \\ M_B^2 = Q^2/N}} \frac{(-Q^2)^N}{\Gamma(N)} \left(\frac{d}{dQ^2}\right)^N \{(-Q^2)^k \Pi(Q^2)\}, \quad (12)$$

at Borel parameter M_B [47–50]. Details on how to evaluate (12) for a correlator such as (10), denoted Π^{QCD} from here on to emphasize that it is a quantity calculated using QCD, can be found in the literature (e.g., [47]). The result is

$$\mathcal{R}_k(M_B) = \int_0^{\infty} t^k e^{-t/M_B^2} \frac{1}{\pi} \text{Im}\Pi^{\text{QCD}}(t) dt \quad (13)$$

for $k \in \{0, 1, 2, \dots\}$ and where

$$\begin{aligned} \frac{1}{\pi} \text{Im}\Pi^{\text{QCD}}(t) = & -A_1 \alpha_s t^3 - A_2 \alpha_s m^2 t^2 \\ & - A_3 \alpha_s t \langle m \bar{q} q \rangle - A_4 t \langle \alpha G^2 \rangle \\ & - A_7 \alpha_s m \langle g \bar{q} \sigma G q \rangle. \end{aligned} \quad (14)$$

Recall, the A_i are given in Table II.

In (11), we impose on $\text{Im}\Pi(t)$ a general resonances-plus-continuum model with onset of the QCD continuum at threshold s_0 ,

$$\text{Im}\Pi(t) = \rho^{\text{had}}(t) + \theta(t - s_0) \text{Im}\Pi^{\text{QCD}}(t), \quad (15)$$

where $\rho^{\text{had}}(t)$ represents the resonance content of the hadronic spectral function and $\theta(t)$ is the Heaviside step function. To isolate the resonance contributions to the LSRs, we consider (continuum-) subtracted LSRs

$$\mathcal{R}_k(M_B, s_0) = \mathcal{R}_k(M_B) - \int_{s_0}^{\infty} t^k e^{-t/M_B^2} \frac{1}{\pi} \text{Im}\Pi^{\text{QCD}}(t) dt. \quad (16)$$

Then, Eqs. (11)–(13), (15), and (16) together imply that

$$\mathcal{R}_k(M_B, s_0) = \int_{t_0}^{\infty} t^k e^{-t/M_B^2} \frac{1}{\pi} \rho^{\text{had}}(t) dt \quad (17)$$

where

$$\mathcal{R}_k(M_B, s_0) = \int_0^{s_0} t^k e^{-t/M_B^2} \frac{1}{\pi} \text{Im}\Pi^{\text{QCD}}(t) dt \quad (18)$$

and (again) $\text{Im}\Pi^{\text{QCD}}(t)$ is given in (14).

There are a number of interesting observations we can make concerning the LSRs of light quarkonium hybrids. In particular, the 6d gluon condensate terms do not contain a logarithm, i.e., $A_6 = 0$ for all J^{PC} values considered (see Table II), and hence do not contribute to the imaginary part (14). This result is surprising: both Diagrams V and VI (see Fig. 1) have logarithmic contributions, but they cancel when the two diagrams are added together. Thus, the LO 6d gluon condensate terms cannot stabilize light quarkonium hybrid LSRs analyses as they have done in some heavy quarkonium hybrid analyses [33–36].

Another observation relates to the mixed condensate contributions. Using (12), if we try to formulate $k = -1$ (i.e., lower-weight) unsubtracted LSRs, we get a piece that formally looks like the right-hand side of (13) at $k = -1$ and another piece:

$$-B_5 \langle \bar{q}q \rangle^2 - B_6 \langle g^3 G^3 \rangle - \left(\frac{A_7}{\epsilon} + B_7 \right) m \langle g \bar{q} \sigma G q \rangle. \quad (19)$$

If $A_7 \neq 0$, then neither piece is well-defined: the integral from (13) diverges and (19) contains a ϵ^{-1} field theory

divergence. But for $J^{PC} \in \{1^{-+}, 1^{++}\}$, we find that $A_7 = 0$ which allows for the construction of lower-weight LSRs in these two channels. Unlike the $k = 0$ LSRs, the $k = -1$ LSRs do receive contributions from the 6d quark and gluon condensates as both B_5 and B_6 are nonzero. An analysis of these $k = -1$ LSRs does require some knowledge of the subtraction constants in (11).

As noted in Sec. I, in the multichannel LSRs analysis of [11], the 0^{+-} , 0^{-+} , 1^{+-} , and 1^{-+} sectors were unstable. The 1^{-+} has since been stabilized using lower-weight LSRs [15], and the 0^{+-} has been stabilized [16] using a different current than that used in [11]. That leaves the non-exotic 1^{+-} and the exotic 0^{+-} channels. Given the GlueX emphasis on exotics and the possible complicated features of mixing between hybrids and conventional quark mesons in the 1^{+-} channel, we focus our attention on 0^{+-} light quarkonium hybrids. Attempts to stabilize the 0^{+-} channel have involved higher-dimension currents combined with lower-weight sum rules requiring estimation of the dispersion-relation low-energy constant within the analysis [13]. Because higher-dimension currents tend to enhance the continuum, the mass determination combined with an estimated low-energy term merits further study.

As in [11], we perform a conventional single narrow resonance (SNR) LSRs analysis of the 0^{+-} channel by letting

$$\rho^{\text{had}}(t) = \pi f^2 \delta(t - m_H^2) \quad (20)$$

in (17) where f is the resonance coupling and m_H is its mass. We include our higher-dimension condensate contributions as well as updated QCD parameter values, yet the analysis remains unstable. The 5d mixed condensate term in the LSRs is small, and, as noted above, the 6d condensates do not contribute at all. In [11], it was suggested that the instability in this channel could be related to a distribution of resonance strength. To investigate this possibility, we use GSRs, an alternative to LSRs which provide a fundamentally different weighting of the hadronic spectral function that makes them well-suited to analyzing distributed resonance strength hadron models. Unsubtracted GSRs of integer weight k are defined as [37]

$$G_k(\hat{s}, \tau) = \sqrt{\frac{\tau}{\pi}} \lim_{\substack{N, \Delta^2 \rightarrow \infty \\ \tau = \Delta^2/(4N)}} \frac{(-\Delta^2)^N}{\Gamma(N)} \left(\frac{d}{d\Delta^2} \right)^N \left\{ \frac{(\hat{s} + i\Delta)^k \Pi(-\hat{s} - i\Delta) - (\hat{s} - i\Delta)^k \Pi(-\hat{s} + i\Delta)}{i\Delta} \right\}. \quad (21)$$

Details on how to evaluate (21) for a correlator such as (10) can be found in [37–39]. The result is

$$G_k(\hat{s}, \tau) = \frac{1}{\sqrt{4\pi\tau}} \int_0^{\infty} t^k e^{-\frac{(\hat{s}-t)^2}{4\tau}} \frac{1}{\pi} \text{Im}\Pi^{\text{QCD}}(t) dt \quad (22)$$

for $k \in \{0, 1, 2, \dots\}$ and where $\frac{1}{\pi} \text{Im}\Pi^{\text{QCD}}(t)$ is given in (14). Subtracted GSRs are defined in much the same way as subtracted LSRs leading to the following GSRs analogues of (17) and (18):

$$G_k(\hat{s}, \tau, s_0) = \frac{1}{\sqrt{4\pi\tau}} \int_{t_0}^{\infty} t^k e^{-\frac{(\hat{s}-t)^2}{4\tau}} \frac{1}{\pi} \rho^{\text{had}}(t) dt \quad (23)$$

where

$$G_k(\hat{s}, \tau, s_0) = \frac{1}{\sqrt{4\pi\tau}} \int_0^{\infty} t^k e^{-\frac{(\hat{s}-t)^2}{4\tau}} \frac{1}{\pi} \text{Im}\Pi^{\text{QCD}}(t) dt. \quad (24)$$

The difference between (17)–(18) and (23)–(24) is in the kernel of the integrals: a decaying exponential for LSRs and a Gaussian for GSRs. The two sum rules represent fundamentally different weightings of the spectral function $\rho^{\text{had}}(t)$; whereas in the LSRs have a duality interval of width $\sim 1/M_B^2$ near the low-energy threshold of the spectral function, the GSRs have a duality interval of width $\sim \sqrt{2\tau}$ near \hat{s} (23). In the $\tau \rightarrow 0^+$ limit, we have

$$\lim_{\tau \rightarrow 0^+} \frac{1}{\sqrt{4\pi\tau}} e^{-\frac{(\hat{s}-t)^2}{4\tau}} = \delta(\hat{s} - t), \quad (25)$$

which, when applied to (23), yields

$$\lim_{\tau \rightarrow 0^+} G_k(\hat{s}, \tau, s_0) = \hat{s}^k \frac{1}{\pi} \rho^{\text{had}}(\hat{s}) \quad \text{for } \hat{s} > t_0. \quad (26)$$

Hence, at least in principle, $\rho^{\text{had}}(t)$ can be extracted directly from GSRs. Realistically, the $\tau \rightarrow 0^+$ limit cannot be achieved, however, because, through renormalization-group (RG) improvement (see Sec. V), the renormalization scale at which α_s is evaluated decreases with decreasing τ [37]. Nevertheless, it is desirable to use low values of τ to minimize the smearing of $\rho^{\text{had}}(t)$ by the kernel of the GSRs. To further emphasize this, we draw upon an analogy introduced in the seminal GSRs paper [37]. Gaussian sum rules satisfy the classical heat equation

$$\frac{\partial^2 G_k(\hat{s}, \tau, s_0)}{\partial \hat{s}^2} = \frac{\partial G_k(\hat{s}, \tau, s_0)}{\partial \tau}, \quad (27)$$

reinterpreting the parameter \hat{s} as ‘‘position,’’ the Gaussian width τ as ‘‘time,’’ and the GSRs $G_k(\hat{s}, \tau, s_0)$ as ‘‘temperature.’’ The smaller the value of τ (i.e., the less time that has passed), the better we may assess the original (i.e., $\tau \rightarrow 0^+$) temperature distribution [i.e., $\hat{s}^k \frac{1}{\pi} \rho^{\text{had}}(\hat{s})$].

Compared to LSRs, GSRs permit greater access to the structure of $\rho^{\text{had}}(t)$. The LSRs methodology is specifically formulated to accentuate the ground state region of the hadronic spectral function while suppressing higher energies. With GSRs, this need not be the case as \hat{s} , the position of the Gaussian kernel’s peak, is a free parameter. By varying \hat{s} , GSRs can probe a wide region of the hadronic spectral function with the same sensitivity as the ground state region. As such, GSRs are generally preferable to LSRs when studying distributed resonance strength models, as demonstrated in the successful analysis of the ρ

meson using GSRs methodology [38]. Integrating (23) with respect to \hat{s} gives

$$\int_{-\infty}^{\infty} G_k(\hat{s}, \tau, s_0) d\hat{s} = \int_{t_0}^{\infty} t^k \frac{1}{\pi} \rho^{\text{had}}(t) dt \quad (28)$$

from which we recognize the quantity on the left-hand side as the finite-energy sum rule of weight k . As shown in [37], a resonance plus continuum model evolved through the diffusion equation only reproduces the QCD prediction at large energy scales if s_0 is constrained by (28). To isolate the information contained in the GSRs formalism that is independent of (28), we consider normalized Gaussian sum rules (NGSRs) [38]

$$N_k(\hat{s}, \tau, s_0) = \frac{G_k(\hat{s}, \tau, s_0)}{M_{k,0}(\tau, s_0)}, \quad (29)$$

i.e., GSRs scaled by their 0th-order moments $M_{k,0}(\hat{s}, \tau)$ where, in general,

$$M_{k,n}(\tau, s_0) = \int_{-\infty}^{\infty} \hat{s}^n G_k(\hat{s}, \tau, s_0) d\hat{s}. \quad (30)$$

Combining (23), (28), and (29), we get a NGSRs analogue of (23),

$$N_k(\hat{s}, \tau, s_0) = \frac{\frac{1}{\sqrt{4\pi\tau}} \int_{t_0}^{\infty} t^k e^{-\frac{(\hat{s}-t)^2}{4\tau}} \frac{1}{\pi} \rho^{\text{had}}(t) dt}{\int_{t_0}^{\infty} t^k \frac{1}{\pi} \rho^{\text{had}}(t) dt}. \quad (31)$$

Finally, to emphasize the low-energy region of the spectral function, we work with the lowest-weight sum rules (i.e., $k = 0$) as in previous applications of GSRs to the prediction of resonance properties [38,39].

IV. HÖLDER INEQUALITY

Previous investigations of hadronic systems using LSRs have employed Hölder inequalities to restrict the set of allowed τ and s_0 values [51–53]. The Hölder Inequality is expressed generally as

$$\left| \int_{t_1}^{t_2} f(t)g(t)d\mu \right| \leq \left(\int_{t_1}^{t_2} |f(t)|^p d\mu \right)^{\frac{1}{p}} \times \left(\int_{t_1}^{t_2} |g(t)|^q d\mu \right)^{\frac{1}{q}} \quad (32)$$

under the condition

$$\frac{1}{p} + \frac{1}{q} = 1 \quad (33)$$

and where $d\mu$ is an arbitrary integration measure. From positivity of the hadronic spectral function for diagonal

correlators, we can use $\text{Im}\Pi^{\text{QCD}}(t) > 0$ to form an integration measure. Substituting this integration measure into (32) leads to restrictions on the allowed values of \hat{s} , τ , and s_0 in the GSRs. We consider the inequality (32) with the assignments

$$d\mu = \text{Im}\Pi^{\text{QCD}}(t)dt \quad (34)$$

$$f(t) = t^\alpha \left(\frac{e^{-\frac{(\hat{s}-t)^2}{4\tau}}}{\sqrt{4\pi\tau}} \right)^a \quad (35)$$

$$g(t) = t^\beta \left(\frac{e^{-\frac{(\hat{s}-t)^2}{4\tau}}}{\sqrt{4\pi\tau}} \right)^b \quad (36)$$

$$t_1 = t_0, \quad t_2 = s_0 \quad (37)$$

$$a + b = 1 \quad (38)$$

where $\alpha + \beta$ is a non-negative integer. Defining

$$\tau_1 = \frac{\tau}{ap} \quad \text{and} \quad \tau_2 = \frac{\tau}{bq}, \quad (39)$$

the inequality (32) becomes

$$G_{\alpha+\beta}(\tau, \hat{s}, s_0) \leq \left(\frac{\tau_1}{\tau} \right)^{\frac{1}{2p}} \left(\frac{\tau_2}{\tau} \right)^{\frac{1}{2q}} \times G_{\alpha p}^{\frac{1}{p}}(\tau_1, \hat{s}, s_0) G_{\beta q}^{\frac{1}{q}}(\tau_2, \hat{s}, s_0) \quad (40)$$

where we have used $G_k(\tau, \hat{s}, s_0) > 0$, the weakest constraint on the GSRs that emerges from positivity of the spectral function. We define ω as follows:

$$\omega = \frac{1}{p} \Leftrightarrow 1 - \omega = \frac{1}{q}, \quad 0 < \omega < 1 \quad (41)$$

and consider (40) with zero-weight GSRs (i.e., $\alpha = \beta = 0$),

$$G_0(\tau, \hat{s}, s_0) \leq \left(\frac{\tau_1}{\tau} \right)^{\frac{\omega}{2}} \left(\frac{\tau_2}{\tau} \right)^{\frac{1-\omega}{2}} G_0^\omega(\tau_1, \hat{s}, s_0) G_0^{1-\omega}(\tau_2, \hat{s}, s_0). \quad (42)$$

Equations (34), (39), and (41) together imply that

$$\tau = \frac{\tau_1 \tau_2}{(1-\omega)\tau_1 + \omega\tau_2} \quad (43)$$

which, when substituted into (42), gives

$$G_0\left(\frac{\tau_1 \tau_2}{(1-\omega)\tau_1 + \omega\tau_2}, \hat{s}, s_0\right) \leq \left(\frac{(1-\omega)\tau_1 + \omega\tau_2}{\tau_2}\right)^{\frac{\omega}{2}} \left(\frac{(1-\omega)\tau_1 + \omega\tau_2}{\tau_1}\right)^{\frac{1-\omega}{2}} G_0^\omega(\tau_1, \hat{s}, s_0) G_0^{1-\omega}(\tau_2, \hat{s}, s_0). \quad (44)$$

Following [53], we set

$$\tau_1 = \tau \quad (45)$$

$$\tau_2 = \tau + \delta\tau \quad (46)$$

which implies

$$0 \leq G_0\left(\frac{\tau(\tau + \delta\tau)}{\omega(\tau + \delta\tau) + (1-\omega)\tau}, \hat{s}, s_0\right) - \left(\frac{\omega(\tau + \delta\tau) + (1-\omega)\tau}{(\tau + \delta\tau)}\right)^{\frac{\omega}{2}} \left(\frac{\omega(\tau + \delta\tau) + (1-\omega)\tau}{\tau}\right)^{\frac{1-\omega}{2}} \times G_0^\omega(\tau, \hat{s}, s_0) G_0^{1-\omega}(\tau + \delta\tau, \hat{s}, s_0). \quad (47)$$

We can perform a local analysis of (47) by expanding about $\delta\tau = 0$,

$$0 \leq \frac{\omega(\omega - 1) \left(1 - 2\tau^2 \left(\frac{G'_0(\hat{s}, \tau, s_0)}{G_0(\hat{s}, \tau, s_0)} \right)^2 + 2\tau \left(2 \left(\frac{G'_0(\hat{s}, \tau, s_0)}{G_0(\hat{s}, \tau, s_0)} \right) + \tau \left(\frac{G''_0(\hat{s}, \tau, s_0)}{G_0(\hat{s}, \tau, s_0)} \right) \right) \right) (\delta\tau)^2}{4\tau^2} + \mathcal{O}((\delta\tau)^3), \quad (48)$$

where primes indicate τ -derivatives. Then, (41) and (48) together imply

$$H(\hat{s}, \tau, s_0) \equiv 1 - 2\tau^2 \left(\frac{G'_0(\hat{s}, \tau, s_0)}{G_0(\hat{s}, \tau, s_0)} \right)^2 + 2\tau \left(2 \left(\frac{G'_0(\hat{s}, \tau, s_0)}{G_0(\hat{s}, \tau, s_0)} \right) + \tau \left(\frac{G''_0(\hat{s}, \tau, s_0)}{G_0(\hat{s}, \tau, s_0)} \right) \right) \geq 0. \quad (49)$$

At some (τ, \hat{s}, s_0) , if the GSR $G_0(\hat{s}, \tau, s_0)$ is to be consistent with a positive hadronic spectral function, then it must satisfy the inequality (49).

V. ANALYSIS METHODOLOGY AND RESULTS

Before we can analyze 0^{+-} light quarkonium hybrids using (31), we need to discuss the QCD parameters appearing in (10), i.e., the coupling, the quark mass, and the QCD condensates.

To implement RG improvement we replace α_s and m in (10) by one-loop, $\overline{\text{MS}}$ running quantities [37]. In our analysis, we use the QCD running coupling anchored at the τ -lepton mass,

$$\alpha_s(\mu) = \frac{\alpha_s(M_\tau)}{1 + \frac{\alpha_s(M_\tau)}{12\pi} (33 - 2n_f) \log(\frac{\mu^2}{M_\tau^2})}, \quad (50)$$

where we use PDG [54] values for the τ mass and

$$\alpha_s(M_\tau) = 0.325 \pm 0.015. \quad (51)$$

For the light quark masses, we use

$$m(\mu) = m(2 \text{ GeV}) \left(\frac{\alpha_s(\mu)}{\alpha_s(2 \text{ GeV})} \right)^{\frac{12}{33-2n_f}}, \quad (52)$$

where

$$m(2 \text{ GeV}) = \frac{1}{2} (m_u(2 \text{ GeV}) + m_d(2 \text{ GeV})) = 3.5_{-0.3}^{+0.7} \text{ MeV} \quad (53)$$

for nonstrange quarks and

$$m(2 \text{ GeV}) = 96_{-4}^{+8} \text{ MeV} \quad (54)$$

for strange quarks [54]. In both (50) and (52), we set $n_f = 4$.

Renormalization-group arguments identify our renormalization scale as $\mu = \tau^{1/4}$ [37,38], putting a lower bound on our choice of τ restricted by the reliability of perturbation theory. A related issue associated with τ is reliability of the GSRs as quantified by the relative contributions of perturbative versus nonperturbative effects and the relative contributions of the resonance versus continuum. We therefore restrict our analysis to $\tau \geq M_\tau$, approximately equivalent to $\tau > 10 \text{ GeV}^4$ as discussed in Sec. V. We also work with an upper bound $\tau \leq 20 \text{ GeV}^4$ emerging from the Hölder inequality constraint (49), as presented in detail in Section V.

Turning to the condensates, the value of the RG-invariant quantity $\langle m\bar{q}q \rangle$ is well-known from PCAC [55]. Using the conventions of [50], we have

$$\langle m\bar{q}q \rangle = \begin{cases} -\frac{1}{2} f_\pi^2 m_\pi^2, & \text{for nonstrange } q \\ -\frac{1}{2} f_K^2 m_K^2, & \text{for strange } q \end{cases} \quad (55)$$

where PDG values are used for the meson masses [54] and the decay constants are [56]

$$f_\pi = (92.2 \pm 3.5) \text{ MeV}, \quad f_K = (110.0 \pm 4.2) \text{ MeV}. \quad (56)$$

We use the following value for the 4d gluon condensate [57]:

$$\langle \alpha G^2 \rangle = (0.075 \pm 0.020) \text{ GeV}. \quad (57)$$

The nonstrange- and strange-flavored 5d mixed condensates are estimated by [58,59] to be

$$\frac{m \langle g\bar{q}\sigma Gq \rangle}{\langle m\bar{q}q \rangle} \equiv M_0^2 = (0.8 \pm 0.1) \text{ GeV}^2. \quad (58)$$

Finally, we note that while the 6d quark and gluon condensates were included in the correlator calculation (10), Table II shows that neither contributes to the $k = 0$ GSRs (24) or NGRs (29).

As noted in Sec. III, a SNR analysis of 0^{+-} light quarkonium hybrids fails within the LSRs methodology, and so we turn our attention to models with distributed resonance strength using GSRs. As confirmation of the consistency between the LSRs and GSRs methodology, we analysed the original stabilizing channels in the LSRs methodology $J^{PC} \in \{0^{\pm\pm}, 1^{\pm\pm}\}$ [11] and found excellent agreement between the results for both mass predictions and continuum onsets. To confirm the need for a distributed resonance model in the case of $J^{PC} = 0^{+-}$, we consider the quantity [39]

$$\sigma_0^2(\tau, s_0) \equiv \frac{M_{0,2}(\tau, s_0)}{M_{0,0}(\tau, s_0)} - \left(\frac{M_{0,1}(\tau, s_0)}{M_{0,0}(\tau, s_0)} \right)^2 \quad (59)$$

where the QCD moments, $M_{k,n}(\tau, s_0)$, were defined in (30). Combining (23) and (59) gives

$$\sigma_0^2(\tau, s_0) = \frac{\int_{t_0}^{\infty} (t^2 + 2\tau) \rho^{\text{had}}(t) dt}{\int_{t_0}^{\infty} \rho^{\text{had}}(t) dt} - \left(\frac{\int_{t_0}^{\infty} t \rho^{\text{had}}(t) dt}{\int_{t_0}^{\infty} \rho^{\text{had}}(t) dt} \right)^2. \quad (60)$$

For a SNR model, substituting (20) into (60) yields

$$\sigma_0^2(\tau, s_0) = 2\tau. \quad (61)$$

Hence, the quantity $\sigma_0^2(\tau, s_0) - 2\tau$ provides a QCD-calculated, model-independent way to assess the suitability of representing a particular hadronic spectral function as a single narrow resonance. If $\sigma_0^2(\tau, s_0) - 2\tau \approx 0$, then a single narrow resonance model is appropriate. On the other hand,

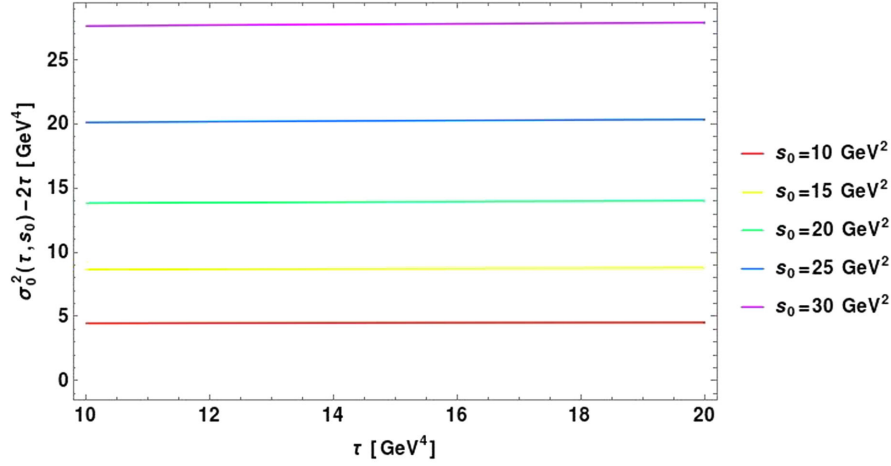


FIG. 2. The QCD prediction for the quantity $\sigma_0^2 - 2\tau$ (where σ_0^2 is defined in (59)) for nonstrange quarks versus τ at several values of the continuum threshold s_0 .

if $\sigma_0^2(\tau, s_0) - 2\tau \approx 0$, then the hadronic spectral function has distributed resonance strength. And so, in Fig. 2, we plot the QCD prediction $\sigma_0^2(\tau, s_0) - 2\tau$ versus τ for nonstrange quarks at several values of s_0 over the range $10 \text{ GeV}^2 \leq s_0 \leq 30 \text{ GeV}^2$. Clearly, $\sigma_0^2(\tau, s_0) - 2\tau \approx 0$, providing further motivation to consider models other than the SNR. An analogous analysis for strange quarks leads to the same conclusion.

If the distributed resonance strength indicated by Fig. 2 is due to a single wide resonance (SWR), then we can determine a rough lower bound on the resonance's width using a rectangular pulse resonance model,

$$\rho^{\text{had}}(t) = \frac{\pi f}{2m_H \Gamma} [\theta(t - m_H^2 + m_H \Gamma) - \theta(t - m_H^2 - m_H \Gamma)], \quad (62)$$

where f is the resonance's coupling, Γ is its width, and m_H is its mass. Substituting (62) into (60) gives

$$\sigma_0^2(\tau, s_0) = 2\tau + \frac{1}{3} m_H^2 \Gamma^2 \quad (63)$$

$$\Rightarrow \Gamma = \frac{1}{m_H} \sqrt{3(\sigma_0^2(\tau, s_0) - 2\tau)}. \quad (64)$$

From (64), we see that Γ decreases as m_H increases. However, to ensure that the resonance does not merge with the continuum, we require

$$m_H^2 + m_H \Gamma < s_0 \quad (65)$$

which implies that the largest possible resonance mass for a particular s_0 is given by

$$m_{H,\text{max}}(\tau, s_0) = \sqrt{s_0 - \sqrt{3(\sigma_0^2(\tau, s_0) - 2\tau)}} \quad (66)$$

where we have used (63). By letting $m_H \rightarrow m_{H,\text{max}}$ in (64), we find that the smallest possible resonance width for a particular s_0 is given by

$$\Gamma_{\text{min}}(\tau, s_0) = \sqrt{\frac{3(\sigma_0^2(\tau, s_0) - 2\tau)}{s_0 - \sqrt{3(\sigma_0^2(\tau, s_0) - 2\tau)}}}. \quad (67)$$

From Fig. 2, we see that $\sigma_0^2(\tau, s_0) - 2\tau$ shows almost no τ -dependence; hence, the same can be said about $\Gamma_{\text{min}}(\tau, s_0)$. In Fig. 3, we plot $\Gamma_{\text{min}}(\tau, s_0)$ versus s_0 at $\tau = 10 \text{ GeV}^4$ for nonstrange quarks. An analogous plot for strange quarks looks nearly identical. At $s_0 = 10 \text{ GeV}^2$, we find that $\Gamma_{\text{min}} \approx 1.46 \text{ GeV}$, far larger than a typical hadron width. As s_0 increases, so too does Γ_{min} . For these reasons, we abandon SWR models in favor of a multi-resonance model.

We consider a double narrow resonance (DNR) model

$$\rho^{\text{had}}(t) = \pi(f_1^2 \delta(t - m_1^2) + f_2^2 \delta(t - m_2^2)), \quad (68)$$

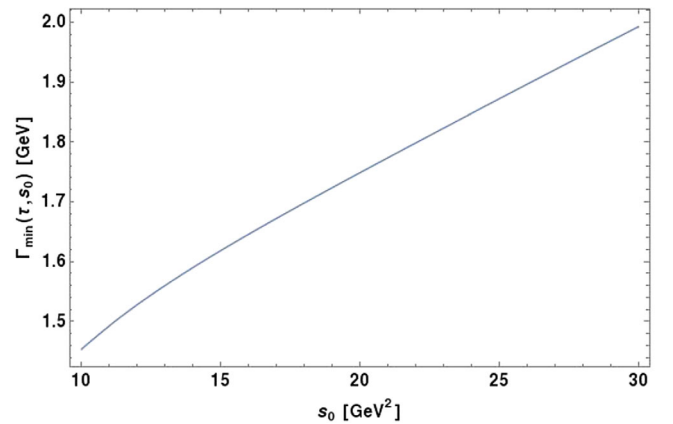


FIG. 3. Minimum rectangular pulse resonance width, Γ_{min} from (67), at $\tau = 10 \text{ GeV}^4$ for nonstrange quarks versus the continuum threshold, s_0 .

where f_1, f_2 and m_1, m_2 are the resonances' couplings and masses respectively. Substituting (68) into (31) gives

$$N_0(\hat{s}, \tau, s_0) = \frac{\left(r e^{-\frac{(s-m_1^2)^2}{4\tau}} + (1-r) e^{-\frac{(s-m_2^2)^2}{4\tau}} \right)}{\sqrt{4\pi\tau}} \quad (69)$$

where

$$r = \frac{f_1^2}{f_1^2 + f_2^2} \Leftrightarrow 1 - r = \frac{f_2^2}{f_1^2 + f_2^2}. \quad (70)$$

At fixed values of τ and s_0 , we perform a fit of (69) over \hat{s} [60] to find best fit parameters for r, m_1 , and m_2 . In Figure 4, we plot the best fit r versus s_0 at $\tau = 10 \text{ GeV}^4$ for nonstrange quarks. Again, an analogous plot for strange quarks looks nearly identical. From the s_0 -stability in r versus s_0 , we determine an optimized continuum onset for both the nonstrange- and strange-flavored cases as

$$s_0^{\text{opt}} = (14.5 \pm 1.2) \text{ GeV}^2 \quad (71)$$

where the uncertainties originate from the QCD input parameters; details of the uncertainty analysis are discussed below. Then, a fit to (69) at $s_0 = 14.5 \text{ GeV}^2$ and $\tau = 10 \text{ GeV}^4$, leads to DNR model parameters

$$r = 0.712 \pm 0.005 \quad (72)$$

$$m_1 = 3.57 \pm 0.15 \text{ GeV} \quad (73)$$

$$m_2 = 2.60 \pm 0.14 \text{ GeV} \quad (74)$$

in the nonstrange-flavored case and

$$r = 0.711 \pm 0.005 \quad (75)$$

$$m_1 = 3.57 \pm 0.13 \text{ GeV} \quad (76)$$

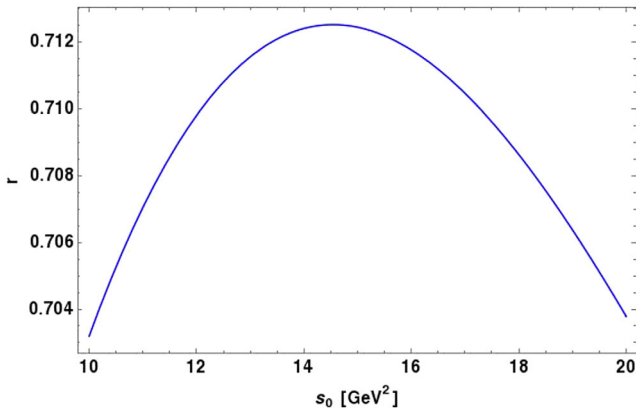


FIG. 4. Plot of the best fit r [defined in (70)] to (69) at $\tau = 10 \text{ GeV}^4$ as a function of continuum threshold, s_0 .

$$m_2 = 2.60 \pm 0.14 \text{ GeV} \quad (77)$$

in the strange-flavored case. Figure 5 shows negligible τ dependence in the mass predictions. Figure 6 shows comparisons between the NGRs and the DNR model [respectively the left- and right-hand sides of (69)] for parameters (72)–(74) at $\tau = 10 \text{ GeV}^4$ and $\tau = 20 \text{ GeV}^4$. We note that the strange and nonstrange 0^{+-} hybrid mass predictions are degenerate within the uncertainties of our analysis; we find this to be consistent with other recent SR analyses [42,61]. We note that the correlator terms that contain the strange quark mass and condensates are numerically small in our calculation, and do not significantly impact the resulting mass prediction. The relatively small numerical difference between strange and nonstrange 0^{+-} hybrids could suggest a dominance of constituent gluonic effects in these systems.

Utilizing the Hölder Inequality test (49), we can perform a consistency check on our analysis. To determine whether (49) is satisfied within the expected uncertainties of the GSRs, we examine the inequality at $s_0^{\text{opt}} = 14.5 \text{ GeV}^2$ for various values of τ . Because our QCD calculations of Wilson coefficients are truncated perturbative series in α_s , in addition to the QCD parameter uncertainties, we use the 1^{-+} channel [62] to provide an estimated next-order perturbative correction characteristic of hybrid correlators. We find that the Hölder inequality constraint (49) is violated for $\tau \gtrsim 20 \text{ GeV}^4$, and the inequality test for the minimum value $\tau = 10 \text{ GeV}^4$ is shown in Fig. 7. Thus, the τ range used in our analysis, $10 \text{ GeV}^4 < \tau < 20 \text{ GeV}^4$, is consistent with the Hölder inequality.

To explore the lower bound on τ in more detail, we consider OPE convergence and resonance dominance in the GSR. As in LSRs, a reliable GSR analysis requires that perturbation theory dominates power-law corrections and that the resonance contributions dominate the continuum. The average relative contribution of the non-perturbative terms is calculated over the region $10 \text{ GeV}^2 - \sqrt{2\tau} < \hat{s} < 10 \text{ GeV}^2 + \sqrt{2\tau}$ to encompass the peak in Fig. 6.

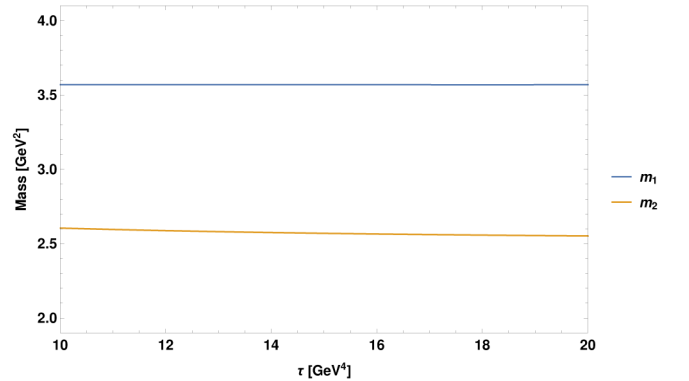


FIG. 5. Plot of 0^{+-} light quarkonium hybrid masses $m_1(\tau, s_0^{\text{opt}})$ and $m_2(\tau, s_0^{\text{opt}})$ of the DNR model (68) at continuum threshold $s_0^{\text{opt}} = 14.5 \text{ GeV}^2$.

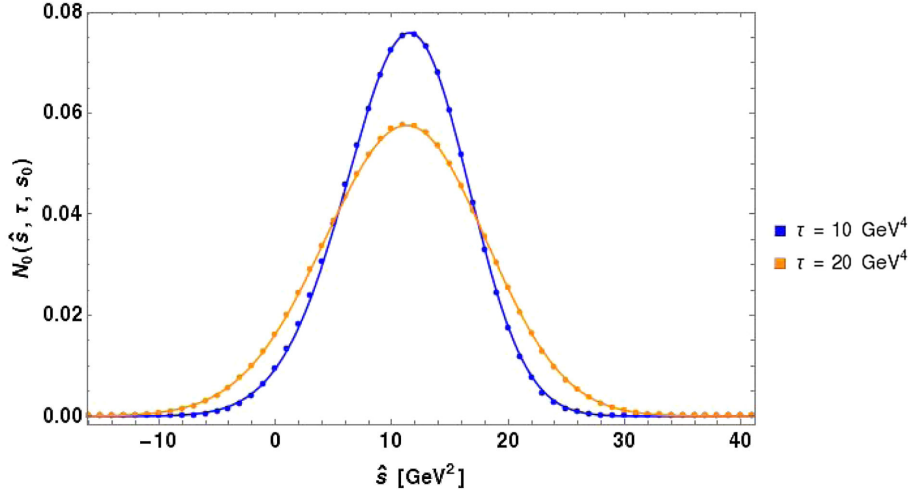


FIG. 6. Comparison of the two sides of (69) for nonstrange DNR parameters (72)–(74) and for $\tau = 10 \text{ GeV}^4$ and $\tau = 20 \text{ GeV}^4$ at $s_0^{\text{opt}} = 14.5 \text{ GeV}^2$. Solid curves correspond to the left-hand side of (69); dots correspond to the right-hand side at selected values of \hat{s} .

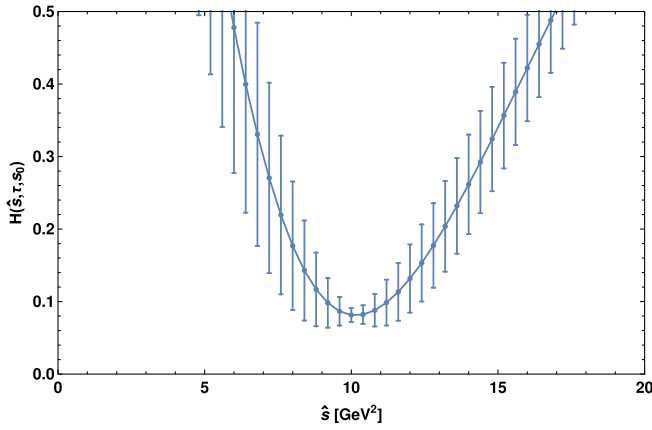


FIG. 7. Plot of inequality test (49) for $\tau = 10 \text{ GeV}^4$ with error bars displayed. Errors are due to variations in the condensate parameters, variations in α_s , and uncertainties in s_0^{opt} (71).

For $\tau = 10 \text{ GeV}^4$, the \hat{s} -averaged nonperturbative contributions are less than 20% of the total and are thus safely controlled. As τ decreases, the relative nonperturbative contribution increases (e.g., to 25% at $\tau = 5 \text{ GeV}^4$). The relative contribution of the resonance versus continuum contribution is much more sensitive to τ . For $\tau = 10 \text{ GeV}^4$ the \hat{s} -averaged ratio of resonance to continuum effects is 50% but for $\tau = 5 \text{ GeV}^4$ the ratio decreases to 30%. We thus conclude that the criteria of OPE convergence and resonance dominance requires $\tau > 10 \text{ GeV}^4$ for a reliable GSR analysis. The combination of the Hölder inequality, OPE convergence, and resonance dominance constrains our GSR window of analysis to $10 \text{ GeV}^4 < \tau < 20 \text{ GeV}^4$.

We verify the s_0 optimization (71) obtained from Fig. 4 by looking at an independent analysis developed in [39] based on the properties of the \hat{s} peak position (maximum)

of the NGRs. For the SNR model (20) the \hat{s} -peak occurs at $\hat{s} = m^2$, independent of τ . Thus, an alternative s_0 -optimization criterion for the SNR is minimizing the τ -dependence of the peak position $\hat{s}_{\text{peak}}(\tau, s_0)$ defined implicitly from

$$\left. \frac{\partial}{\partial \hat{s}} N_0^{\text{QCD}}(\hat{s}, \tau, s_0) \right|_{\hat{s}=\hat{s}_{\text{peak}}(\tau, s_0)} = 0. \quad (78)$$

For the DNR model (68), the peak position acquires τ -dependence modeled by

$$\hat{s}_{\text{peak}}(\tau, s_0) = A + \frac{B}{\tau} + \frac{C}{\tau^2} + \frac{D}{\tau^3} \quad (79)$$

where the unknown parameters $\{A, B, C, D\}$ are constrained by minimizing the χ^2

$$\chi^2(A, B, C, D, s_0) = \sum_{\tau=10 \text{ GeV}^4}^{20 \text{ GeV}^4} \left(\frac{A + \frac{B}{\tau} + \frac{C}{\tau^2} + \frac{D}{\tau^3}}{\hat{s}_{\text{peak}}(\tau, s_0)} - 1 \right)^2. \quad (80)$$

By minimizing (80) with respect to A, B, C, D , and s_0 , we find an optimum continuum threshold $s_0^{\text{opt}} = 14.0 \text{ GeV}^2$ in excellent agreement with the value obtained in (71).

To obtain errors in s_0^{opt} , r , m_1 , and m_2 , we examine how the errors in the QCD parameters impact the values of these optimized parameters by varying each independently and examining the impact on the model parameters. Additionally, there exists a methodological error in determining s_0^{opt} as the variance in the QCD parameters will affect the stability point of r . Contributions to the error in s_0^{opt} are summarized in Table IV and contributions to the error in the DNR model parameters are summarized in Tables V–VII. The dominant error in s_0^{opt} comes from the variation in $\langle \alpha G^2 \rangle$; in determining errors in the DNR

TABLE IV. Contributions to s_0^{opt} error at $\tau = 10 \text{ GeV}^4$ due to variations in QCD parameter error. Columns $\pm\delta$ indicate variations in DNR parameters at the upper ($+\delta$) and lower ($-\delta$) bounds of the corresponding QCD parameters.

Error source	Nonstrange		Strange	
	$+\delta$	$-\delta$	$+\delta$	$-\delta$
$\langle m\bar{q}q \rangle$	5.62×10^{-3}	-6.74×10^{-4}	9.38×10^{-3}	3.09×10^{-3}
$\langle \alpha G^2 \rangle$	-9.20×10^{-1}	1.18×10^0	-9.16×10^{-1}	1.18×10^0
$\langle g\bar{q}\sigma Gq \rangle$	1.11×10^{-4}	1.00×10^{-3}	3.66×10^{-3}	4.77×10^{-3}
α_s	1.70×10^{-1}	-1.86×10^{-1}	1.74×10^{-1}	-1.82×10^{-1}

TABLE V. Contributions to r error at $\tau = 10 \text{ GeV}^4$ due to variations in QCD parameter error. Columns $\pm\delta$ indicate variations in DNR parameters at the upper ($+\delta$) and lower ($-\delta$) bounds of the corresponding QCD parameters.

Error source	Nonstrange		Strange	
	$+\delta$	$-\delta$	$+\delta$	$-\delta$
$\langle m\bar{q}q \rangle$	-2.86×10^{-6}	2.76×10^{-6}	-2.58×10^{-6}	3.04×10^{-6}
$\langle \alpha G^2 \rangle$	4.79×10^{-3}	-4.66×10^{-3}	4.79×10^{-3}	-4.66×10^{-3}
$\langle g\bar{q}\sigma Gq \rangle$	1.43×10^{-6}	-1.34×10^{-6}	1.70×10^{-6}	-1.06×10^{-6}
α_s	-7.93×10^{-4}	8.73×10^{-4}	-7.93×10^{-4}	8.73×10^{-4}
s_0^{opt}	5.09×10^{-4}	3.53×10^{-4}	3.57×10^{-4}	4.81×10^{-4}

TABLE VI. Contributions to m_1 error at $\tau = 10 \text{ GeV}^4$ due to variations in QCD parameter error. Columns $\pm\delta$ indicate variations in DNR parameters at the upper ($+\delta$) and lower ($-\delta$) bounds of the corresponding QCD parameters.

Error source	Nonstrange		Strange	
	$+\delta$	$-\delta$	$+\delta$	$-\delta$
$\langle m\bar{q}q \rangle$	-6.84×10^{-6}	6.58×10^{-6}	-7.06×10^{-6}	6.35×10^{-6}
$\langle \alpha G^2 \rangle$	5.79×10^{-3}	-7.02×10^{-3}	5.79×10^{-3}	-7.02×10^{-3}
$\langle g\bar{q}\sigma Gq \rangle$	-3.07×10^{-6}	3.01×10^{-6}	-3.29×10^{-6}	2.79×10^{-6}
α_s	-1.06×10^{-3}	1.13×10^{-3}	-1.06×10^{-3}	1.13×10^{-3}
s_0^{opt}	1.48×10^{-1}	-1.21×10^{-1}	1.49×10^{-1}	-1.20×10^{-1}

TABLE VII. Contributions to m_2 error at $\tau = 10 \text{ GeV}^4$ due to variations in QCD parameter error. Columns $\pm\delta$ indicate variations in DNR parameters at the upper ($+\delta$) and lower ($-\delta$) bounds of the corresponding QCD parameters.

Error source	Nonstrange		Strange	
	$+\delta$	$-\delta$	$+\delta$	$-\delta$
$\langle m\bar{q}q \rangle$	-3.72×10^{-5}	3.58×10^{-5}	-3.79×10^{-5}	3.51×10^{-5}
$\langle \alpha G^2 \rangle$	2.81×10^{-2}	-3.64×10^{-2}	2.81×10^{-2}	-3.64×10^{-2}
$\langle g\bar{q}\sigma Gq \rangle$	-2.01×10^{-5}	1.99×10^{-5}	-2.08×10^{-5}	1.93×10^{-5}
α_s	-5.36×10^{-3}	5.63×10^{-3}	-5.36×10^{-3}	5.63×10^{-3}
s_0^{opt}	1.40×10^{-1}	-1.12×10^{-1}	1.40×10^{-1}	-1.11×10^{-1}

parameters, the error in r is driven by the variation in $\langle \alpha G^2 \rangle$ while the dominant errors in the masses m_1 and m_2 arise from variations in s_0^{opt} , followed by $\langle \alpha G^2 \rangle$. Errors in $\langle \bar{q}q \rangle$ and $\langle g\bar{q}\sigma Gq \rangle$ contribute negligibly in the error of all DNR

parameters. Adding the values summarized in Tables IV–VII in quadrature gives us a conservative error estimate summarized in Table VIII; as the driving errors in each parameter are approximately equivalent for the upper and lower bounds

TABLE VIII. Calculated total errors in s_0^{opt} , r , m_1 , m_2 from contributions in Tables IV–VII.

Parameter	Value	
	Nonstrange	Strange
s_0^{opt}	$14.5^{+1.2}_{-0.9}$	$14.5^{+1.2}_{-0.9}$
r	0.712 ± 0.005	0.711 ± 0.005
m_1	$3.57^{+0.15}_{-0.12}$	$3.57^{+0.13}_{-0.12}$
m_2	$2.60^{+0.14}_{-0.12}$	$2.60^{+0.14}_{-0.12}$

of the corresponding QCD parameters, we express our DNR parameters (71)–(77) with symmetric error, taking the most conservative bound.

VI. DISCUSSION

We have calculated 5d and 6d QCD condensate contributions to all spin-0 and spin-1 light quarkonium hybrid correlators with the goal of obtaining QCD LSRs mass predictions in the previously-unstable channels of [11]. However, the 6d gluon and quark condensate contributions do not have an imaginary part and hence do not contribute to the LSRs. Also, the 5d mixed condensate contributions turn out to be small. We therefore focused on the suggestion of Refs. [11,13] that a distribution of resonance strength could be the source of instability, a scenario ideally suited to GSRs methods [37–39]. The 0^{+-} channel was chosen for detailed investigation because of its phenomenological significance in light of the GlueX experiment. Furthermore, a model-independent analysis of the 0^{+-} hadronic spectral function implies that there is a distribution of resonance strength in this channel.

In examining the SWR (62) and DNR (68) models, we found that the DNR model provided excellent agreement between QCD and phenomenology. (See Fig. 6.) The SWR model was rejected on the basis of an atypically large resonance width. In the DNR model, we find degenerate

predictions in the case of both nonstrange and strange quark states from the 0^{+-} current: a 2.60 ± 0.14 GeV state (2.60 ± 0.14 GeV in the strange case) with 29% relative coupling, and a state at 3.57 ± 0.15 GeV (3.57 ± 0.13 GeV) with 71% relative coupling. The smaller coupling of the light state suggests the possibility of mixing with a tetraquark because the expected tetraquark mass range is above 2 GeV [63].

The lighter state is consistent with recent lattice results that find a predominantly nonstrange state around 2.4 GeV and a predominantly strange state around 2.5 GeV in the 0^{+-} channel with $m_\pi = 391$ MeV [25]. Our lighter-state mass determination is somewhat larger than the 2.1–2.5 GeV range of central values in [13]. The literature does not provide a clear interpretation of the heavier 0^{+-} state; however lattice studies [25] of the lightest hybrid meson supermultiplet suggest that the 0^{+-} state exists as part of an excited hybrid supermultiplet with radially-excited $q\bar{q}$ pair (i.e., quark total angular momentum $L_{q\bar{q}} = 1$). We suggest that this heavier second state arising in the GSRs is a manifestation of an excited hybrid state.

In conclusion, we investigated light quarkonium, exotic ($J^{PC} = 0^{+-}$) hybrid mesons with SWR and DNR models using a GSRs analysis. We disfavored the SWR model as the predicted resonance width was too large. The double-narrow resonance model yielded two 0^{+-} hybrid states: (2.60 ± 0.14) GeV and (3.57 ± 0.15) GeV ((2.60 ± 0.14) GeV and (3.57 ± 0.13) GeV in the strange case). Additionally, we explored using the Hölder inequality derived for the GSRs as a consistency check on our analysis.

ACKNOWLEDGMENTS

We are grateful for financial support from the Natural Sciences and Engineering Research Council of Canada (NSERC), and the Chinese National Youth Thousand Talents Program.

-
- [1] R. L. Jaffe and K. Johnson, *Phys. Lett.* **60B**, 201 (1976).
 - [2] R. Aaij *et al.*, *Phys. Rev. Lett.* **112**, 222002 (2014).
 - [3] Z. Q. Liu *et al.*, *Phys. Rev. Lett.* **110**, 252002 (2013).
 - [4] M. Ablikim *et al.*, *Phys. Rev. Lett.* **110**, 252001 (2013).
 - [5] R. Aaij *et al.*, *Phys. Rev. Lett.* **115**, 072001 (2015).
 - [6] H. Al Ghouli *et al.*, *AIP Conf. Proc.* **1735**, 020001 (2016).
 - [7] I. I. Balitsky, D. Diakonov, and A. V. Yung, *Phys. Lett.* **112B**, 71 (1982).
 - [8] J. Govaerts, F. de Viron, D. Gusbin, and J. Weyers, *Phys. Lett.* **128B**, 262 (1983); **136B**, 445(E) (1984).
 - [9] J. Govaerts, F. de Viron, D. Gusbin, and J. Weyers, *Nucl. Phys.* **B248**, 1 (1984).
 - [10] J. I. Latorre, S. Narison, P. Pascual, and R. Tarrach, *Phys. Lett.* **147B**, 169 (1984).
 - [11] J. Govaerts, L. Reinders, and J. Weyers, *Nucl. Phys.* **B262**, 575 (1985).
 - [12] I. I. Balitsky, D. Diakonov, and A. V. Yung, *Z. Phys. C* **33**, 265 (1986).
 - [13] V. Braun and A. Kolesnichenko, *Phys. Lett.* **175B**, 485 (1986).
 - [14] J. Govaerts, L. J. Reinders, P. Francken, X. Gonze, and J. Weyers, *Nucl. Phys.* **B284**, 674 (1987).
 - [15] J. I. Latorre, P. Pascual, and S. Narison, *Z. Phys. C* **34**, 347 (1987).

- [16] T. Huang, H. Jin, and A. Zhang, *Eur. Phys. J. C* **8**, 465 (1999).
- [17] K. Chetyrkin and S. Narison, *Phys. Lett. B* **485**, 145 (2000).
- [18] H. Y. Jin and J. G. Korner, *Phys. Rev. D* **64**, 074002 (2001).
- [19] H. Y. Jin, J. G. Korner, and T. G. Steele, *Phys. Rev. D* **67**, 014025 (2003).
- [20] S. Narison, *Phys. Lett. B* **675**, 319 (2009).
- [21] Z. Zhu-Feng, J. Hong-Ying, and T. G. Steele, *Chin. Phys. Lett.* **31**, 051201 (2014).
- [22] Z.-R. Huang, H.-Y. Jin, and Z.-F. Zhang, *J. High Energy Phys.* **04** (2015) 4.
- [23] Z.-R. Huang, H.-Y. Jin, T. G. Steele, and Z.-F. Zhang, *Phys. Rev. D* **94**, 054037 (2016).
- [24] J. J. Dudek, *Phys. Rev. D* **84**, 074023 (2011).
- [25] J. J. Dudek, R. G. Edwards, P. Guo, and C. E. Thomas, *Phys. Rev. D* **88**, 094505 (2013).
- [26] C. J. Burden, L. Qian, C. D. Roberts, P. C. Tandy, and M. J. Thomson, *Phys. Rev. C* **55**, 2649 (1997).
- [27] C. J. Burden and M. A. Pichowsky, *Few Body Syst.* **32**, 119 (2002).
- [28] T. Hilger, M. Gómez-Rocha, and A. Krassnigg, *Eur. Phys. J. C* **77**, 625 (2017).
- [29] F. E. Close and P. R. Page, *Nucl. Phys.* **B443**, 233 (1995).
- [30] T. Barnes, F. E. Close, and E. S. Swanson, *Phys. Rev. D* **52**, 5242 (1995).
- [31] T. Barnes and F. E. Close, *Phys. Lett.* **116B**, 365 (1982).
- [32] M. S. Chanowitz and S. R. Sharpe, *Nucl. Phys.* **B222**, 211 (1983); **B228**, 588(E) (1983).
- [33] C.-F. Qiao, L. Tang, G. Hao, and X.-Q. Li, *J. Phys. G* **39**, 015005 (2012).
- [34] R. Berg, D. Harnett, R. T. Kleiv, and T. G. Steele, *Phys. Rev. D* **86**, 034002 (2012).
- [35] W. Chen, R. T. Kleiv, T. G. Steele, B. Bulthuis, D. Harnett, J. Ho, T. Richards, and S.-L. Zhu, *J. High Energy Phys.* **09** (2013) 19.
- [36] W. Chen, T. G. Steele, and S.-L. Zhu, *J. Phys. G* **41**, 025003 (2014).
- [37] R. Bertlmann, G. Launer, and E. de Rafael, *Nucl. Phys.* **B250**, 61 (1985).
- [38] G. Orlandini, T. G. Steele, and D. Harnett, *Nucl. Phys.* **A686**, 261 (2001).
- [39] D. Harnett and T. G. Steele, *Nucl. Phys.* **A695**, 205 (2001).
- [40] A. Zhang and T. G. Steele, *Nucl. Phys.* **A728**, 165 (2003).
- [41] D. Harnett, R. Kleiv, K. Moats, and T. G. Steele, *Nucl. Phys.* **A850**, 110 (2011).
- [42] J. Ho, D. Harnett, and T. G. Steele, *J. High Energy Phys.* **05** (2017) 149.
- [43] D. Binosi and L. Theußl, *Comput. Phys. Commun.* **161**, 76 (2004).
- [44] R. Mertig and R. Scharf, *Comput. Phys. Commun.* **111**, 265 (1998).
- [45] O. V. Tarasov, *Phys. Rev. D* **54**, 6479 (1996).
- [46] O. V. Tarasov, *Nucl. Phys.* **B502**, 455 (1997).
- [47] M. A. Shifman, A. I. Vainshtein, and V. I. Zakharov, *Nucl. Phys.* **B147**, 385 (1979).
- [48] M. A. Shifman, A. I. Vainshtein, and V. I. Zakharov, *Nucl. Phys.* **B147**, 448 (1979).
- [49] L. J. Reinders, H. Rubinstein, and S. Yazaki, *Phys. Rep.* **127**, 1 (1985).
- [50] S. Narison, *QCD as a Theory of Hadrons: From Partons to Confinement* (Cambridge University Press, Cambridge, England, 2004).
- [51] Q.-N. Wang, Z.-F. Zhang, T. G. Steele, H.-Y. Jin, and Z.-R. Huang, *Chin. Phys. C* **41**, 074107 (2017).
- [52] F. Shi, T. G. Steele, V. Elias, K. Sprague, Y. Xue, and A. Fariborz, *Nucl. Phys.* **A671**, 416 (2000).
- [53] M. Benmerrouche, G. Orlandini, and T. G. Steele, *Phys. Lett. B* **366**, 354 (1996).
- [54] C. Patrignani *et al.* (Particle Data Group), *Chin. Phys. C* **40**, 100001 (2016).
- [55] M. Gell-Mann, R. J. Oakes, and B. Renner, *Phys. Rev. D* **175**, 2195 (1968).
- [56] J. L. Rosner, S. Stone, and R. S. Van de Water, *arXiv*: 1509.02220.
- [57] S. Narison, *Phys. Lett. B* **707**, 259 (2012).
- [58] M. Beneke and H. Dosch, *Phys. Lett. B* **284**, 116 (1992).
- [59] B. Ioffe and V. M. Belyaev, *J. Exp. Theor. Phys.* **56**, 493 (1982).
- [60] using the Mathematica v11 command `NonlinearModelFit`, <https://reference.wolfram.com/language/ref/NMinimize.html>.
- [61] W. Chen, H.-X. Chen, X. Liu, T. G. Steele, and S.-L. Zhu, *Phys. Rev. D* **96**, 114017 (2017).
- [62] H. Y. Jin and J. G. Körner, *Phys. Rev. D* **64**, 074002 (2001).
- [63] D. Meng-Lin, C. Wei, C. Xiao-Lin, and Z. Shi-Lin, *Chin. Phys. C* **37**, 033104 (2013).